



Search for the SM Higgs boson in the $\tau^+\tau^- + 2$ jets final state

The DØ Collaboration
URL: <http://www-d0.fnal.gov>

(Dated: March 11, 2011)

We search for the standard model Higgs boson (H) using 4.3 fb^{-1} of data from the DØ experiment at the Fermilab $p\bar{p}$ collider. We consider nine production and decay final states to which the final state e or μ , a hadronically decaying τ plus two jets can contribute. We consider contributions from two decay channels $H \rightarrow \tau\tau$ and $H \rightarrow WW$. For either decay, we consider the production of H bosons through gluon-gluon, electroweak boson-boson fusion, or Higgs boson production in association with either W or Z . This analysis does not use b -tagging. We construct a set of boosted decision trees whose outputs characterize the difference between specific signal and background processes, and combine the information from these trees in a final combined boosted decision tree to achieve discrimination between the sum of all signals relative to all backgrounds. Combining both the electron and muon channels, and including a previous DØ measurement with 1.0 fb^{-1} of data, we set a 95% CL. limit on the measured H cross sections for $M_H = 110, 130$ and 160 GeV that are factors of 20, 24 and 11 larger than expectations from the standard model, respectively.

Preliminary Results for Winter 2011 Conferences

I. INTRODUCTION

We present a search for the standard model (SM) Higgs boson (H) in final states with a lepton ($\ell \equiv e$ or μ), a candidate for the decay of $\tau \rightarrow$ hadrons $+\nu_\tau$, and two jets. We refer these two final state signatures as the $e\tau jj$ or $\mu\tau jj$ channels, and analyze such events for contributions from :

$$q\bar{q} \rightarrow H(\rightarrow b\bar{b})Z(\rightarrow \tau\tau) \quad (\text{denoted } HZ) \quad (1)$$

$$q\bar{q} \rightarrow ZH \quad (ZH) \quad (2)$$

$$q\bar{q} \rightarrow WH \quad (WH) \quad (3)$$

$$gg \rightarrow H + (\geq 2 \text{ jets}) \quad (\text{gluon gluon fusion, GGF}) \quad (4)$$

$$q\bar{q}' \rightarrow q\bar{q}'H \quad (\text{virtual vector boson fusion, VBF}) \quad (5)$$

The ZH , WH , GGF and VBF production processes are sought both through the $H \rightarrow \tau\tau$ and $H \rightarrow W^+W^-$ decays. For clarity, we refer to subprocesses involving $H \rightarrow \tau\tau$ or $H \rightarrow WW$ as, for example, $WH_{\tau\tau}$ or WH_{WW} . For the VH_{WW} subprocesses ($V = W$ or Z) decays, the lepton can be produced either directly from $W \rightarrow \ell\nu$ or $Z \rightarrow \ell\ell$ with one ℓ not detected, or through V decays to τ lepton states with subsequent decay $\tau \rightarrow \ell\nu\bar{\nu}$. We ignore the signal process $H \rightarrow ZZ$ as it contributes only a small fraction relative to $H \rightarrow WW$. Since most of the signal processes involve light-quark jets in the final state, we do not require b -tagging in this analysis.

The backgrounds to the $\tau(\ell)$ $\tau(\text{hadronic})$ jet jet signatures are from $t\bar{t}$, $W+$ jets, $Z+$ jets, multijets and diboson ($WW/WZ/ZZ$) production.

We use 4.3 fb^{-1} of data collected with the upgraded DØ detector. For the $\mu\tau jj$ final state, our analysis parallels the preselection used in the previous search with 1 fb^{-1} [1]. The current analysis supercedes an earlier preliminary result [2] and adds the $e\tau jj$ final state. Boosted decision trees (BDT) are trained to distinguish individual signal processes from each of the major backgrounds. These individual BDTs are combined in a final combined BDT (cBDT) for three regions of Higgs-boson mass (M_H) to optimize discrimination of the sum of all signals from the sum of all backgrounds. These cBDT distributions are used for setting limits on Higgs boson production.

II. DATA AND MONTE CARLO EVENT SAMPLES

A. DØ Detector

The DØ detector [3, 4] contains tracking, calorimeter and muon subdetector systems. Silicon microstrip tracking detectors (SMT) near the interaction point cover pseudorapidity $|\eta| < 3$ and provide precise tracking and vertexing information. A central fiber tracker surrounds the SMT, providing coverage up to about $|\eta| = 2$. A 2 T solenoid surrounds these tracking detectors. Three uranium liquid-argon calorimeters measure particle energies. The central calorimeter (CC) covers $|\eta| < 1$, and two end calorimeters (EC) extend coverage to about $|\eta| = 4$. Intercryostat detectors provide added sampling in the region $1.1 < |\eta| < 1.4$ where the CC and EC cryostat walls degrade the energy resolution. Muons are measured in stations that use scintillation counters and several layers of tracking chambers over the range $|\eta| < 2$. One station is located just outside the calorimeters, and two more are outside of 1.8 T iron toroidal magnets. Scintillators surrounding the exiting beams are used to determine the instantaneous luminosity. A three-level trigger system selects events for data logging at about 100 Hz.

B. Trigger

The $\mu\tau jj$ data was collected using all triggers operating in DØ. This enhanced the yields by about 45% over those from the suite of single-muon triggers. The acceptance ratio for all triggers relative to the single-muon triggers is calculated from data within the kinematic region appropriate to the single-muon triggers. The single-muon trigger efficiency is parametrized as a function of muon azimuthal angle ϕ and pseudorapidity η . We find no significant dependence of the ratio of all triggers to single-muon triggers on the p_T or η of reconstructed objects (μ , τ or jets) and parametrize the all trigger to single-muon trigger ratio as a constant. The combined efficiency factors are used to weight simulated Monte Carlo (MC) events. The $e\tau jj$ data was collected with a set of triggers sensitive to single electromagnetic objects. For both channels the luminosity was computed using a high transverse momentum jet trigger that was not prescaled in the course of data taking.

C. Monte Carlo samples

The MC samples for the Higgs signal are generated with PYTHIA [5] using CTEQ6L1 [6] leading-order parton distribution functions (PDF). The signal cross sections are normalized to the next-to-next-to-leading order (NNLO) (or NLO for VBF) calculations using results in Ref. [7]. The SM backgrounds from $t\bar{t}$ and V +jets production are generated using ALPGEN [8] with parton showering and hadronization provided by PYTHIA. Production of electroweak VV pairs is generated with PYTHIA. Higgs and τ decays are simulated by HDECAY [9] and TAUOLA [10] respectively. The SM backgrounds $t\bar{t}$ and V +light jets only are normalized to NLO cross sections from the MCFM program [11] and data. The NLO cross sections for dibosons are taken from MCFM.

The SM signals and backgrounds are processed using the standard DØ GEANT3 [12] detector simulation, digitization and event-reconstruction programs. Data events selected randomly using an unbiased beam-crossing trigger are added to the MC events, with a reweighting to account for the observed distribution of the instantaneous luminosity. We also apply a reweighting of MC events to account for mismodelling of p_T^W and p_T^Z in MC.

D. Object identification and event preselection

Muons are identified using hits in the muon scintillator detectors and tracking chambers that are matched to trajectories reconstructed in the central tracker. We place requirements on the number of muon hits in different detector planes, the central track quality and the distance of closest approach between the muon track and the primary interaction vertex. We require $p_T^\mu > 15$ GeV and $|\eta_\mu| < 1.6$. For the signal sample, we impose two muon isolation requirements: the sum of transverse energies deposited within an annular ring around the muon track of $0.1 \leq \mathcal{R} \leq 0.4$ in the calorimeter must be less than 2.5 GeV, and the sum of track transverse momenta, excluding the muon, within a cone $\mathcal{R} \leq 0.5$ around the muon direction must be less than 2.5 GeV, where $\mathcal{R} = \sqrt{(\Delta\phi)^2 + (\Delta\eta)^2}$ is the distance in η - ϕ space. Muons in MC are reweighted as a function of the primary vertex location and their pseudorapidity relative to the detector center to correct mismodelling between MC and data.

Electrons are identified using the distribution and correlation of energy depositions in the electromagnetic (EM) section of the calorimeter, the quality of a match to a central track, the ratio of calorimeter energy to track momentum (expected to be near unity), the fraction of total calorimeter energy deposited in the EM section, and an isolation criterion based on energy in the annular cone $0.1 \leq \mathcal{R} \leq 0.4$ around the track. We form a likelihood function involving all these variables and accepted electrons are required to pass a selection on the likelihood value.

A τ decaying to hadrons is identified using the neural-network procedure given in Ref. [13]. This employs (i) calorimeter clusters found with a simple cone algorithm using $\mathcal{R} = 0.3$; (ii) energy in an annular cone $0.3 \leq \mathcal{R} \leq 0.5$; (iii) electromagnetic (EM) subclusters, and (iv) the multiplicity of tracks with $p_T > 1.5$ GeV within $\mathcal{R} < 0.5$ of the direction of the τ lepton (defined by its visible decay products) and small invariant mass consistent with expectation for τ decays. Neural networks, NN_τ , are used to identify three types of τ decays, (1) $\tau^\pm \rightarrow \pi^\pm\nu$, (2) $\tau^\pm \rightarrow \pi^\pm\pi^0\nu$ and (3) $\tau^\pm \rightarrow \pi^\pm\pi^\pm\pi^\mp(\pi^0)\nu$. A separate NN_τ is constructed for each type. In addition, a neural network NN_{el} is formed to distinguish between type 2 taus and electrons, which have similar signatures. The transverse momentum of the τ , p_T^τ , is computed from the calorimetric energy within the τ cone, improved by the measured track momenta for type 2 and 3 taus. For type 1, p_T^τ is obtained from measured track momentum. We require $p_T^\tau > 12.5$ GeV for types 1 and 2, and > 15 GeV for type 3. The τ candidates are required to have $|\eta| < 2$, measured with respect to the center of the detector. We require the sum of the transverse momenta of the τ -associated tracks, p_T^{trk} , to exceed 5 (10) GeV for τ type 2 (3). In addition, for type 3 τ s, we require at least one track with $p_T > 7$ GeV. A type 3 τ must have at least two reconstructed tracks; if only two are present we require that they be of the same charge so as to give unambiguous determination of the sign of the τ charge. A τ candidate is required to have $p_T^{\text{trk}}/E_T^\tau > (0.65, 0.5, 0.5)$ for τ types (1, 2, 3). The direction of the τ must extrapolate to the primary vertex along the beam direction to within 1.5 cm. To be considered as a τ candidate for a signal process, NN_τ is required to exceed 0.9 for types 1 and 2 and 0.95 for type 3.

Jets are reconstructed using an iterative midpoint cone algorithm [14] with a cone size of $\mathcal{R} = 0.5$. We require at least two tracks in a jet that point to the event primary vertex. Jets are corrected for energy response at the particle level and the imbalance for the muon and missing neutrino energy when there is an indication of semi-muonic decays within the jet. We correct jet objects in the MC for differences between data and MC in identification efficiency and energy resolution. We require jet $p_T > 15$ GeV, the highest p_T jet to have $p_T > 20$ GeV and $|\eta| < 3.4$. The missing transverse energy is calculated as $\cancel{E}_T = \sqrt{(\sum_j E_{x,j})^2 + (\sum_j E_{y,j})^2}$, where $E_{x,j}$ ($E_{y,j}$) is the energy in the j -th calorimeter cell multiplied by $\sin\theta \cos\phi_j$ ($\sin\theta \sin\phi_j$) with ϕ_j being the azimuthal angle of the j -th cell and θ the polar angle, applying standard energy corrections to all cells that belong to all reconstructed objects, including any observed muons. The event \cancel{E}_T is ascribed to the neutrinos from the two τ decays, shared in proportion to the transverse and

longitudinal momenta of their visible decay products, and is used to calculate the $\tau\tau$ invariant mass, and the $e\nu$, $\mu\nu$ or $\tau\nu$ transverse masses.

With the above object definitions, we select a sample of candidate events with the following requirements:

- One isolated lepton, e or μ ;
- At least two jets;
- At least one $\tau \rightarrow$ hadrons candidate. If there is more than one tau candidate, we select the one with the highest p_T^τ ;
- ℓ and τ of opposite electric charge;
- Leptons, taus and jets all separated from each other by $\Delta\mathcal{R} > 0.5$; and
- To assure orthogonality to other H searches, we require no additional electron with $p_T > 12$ (15) GeV and no additional muon with $p_T > 10$ (12) GeV for the $\mu\tau jj$ ($e\tau jj$) channels, respectively. We also require no isolated tracks in the $\mu\tau jj$ analysis which could lead to that event being selected for an independent $Z(\rightarrow \mu + \text{track}) + H$ search [15].

For the $e\tau jj$ analysis, the above selections yield a substantial background contribution from $Z(\rightarrow ee) + \text{jets}$. Therefore we impose the additional requirements on τ 's:

- Remove τ candidates that have 1.05 (1.1) $< \eta < 1.5$ for type 1 (type 3) τ 's. This region between calorimeter cryostats has impaired EM energy response;
- Remove type 2 τ candidates with $\text{NN}_{\text{el}} < 0.95$;
- Remove type 2 τ candidates whose track points to within 10% of either edge of a central calorimeter module in ϕ (where EM energy response is degraded); and
- Remove type 3 τ candidates for which the calorimeter energy in the EM section is more than 95% of the total.

If a τ is removed through these requirements, a second un-vetoed τ candidate is retained in the sample, if available.

To reduce the multijet background in the $e\tau jj$ analysis we require that a measure of the significance of the \cancel{E}_T , \mathcal{S} [16], satisfy $\mathcal{S} > 1$. Events with small \mathcal{S} are mainly due to mismeasurements of jet energies.

Our final selection of signal sample consists of only one lepton (e or μ), one selected hadronic tau, and two good jets. We require the lepton and tau have opposite charge.

E. Estimation of background from multijet events

Multijet (MJ) events in which jets mimic electrons, muons or taus are not reliably simulated in our MC, and are estimated with data-driven techniques. We select a baseline MJ background sample in which both the τ and lepton selections are modified. For the τ , we require $0.3 < \text{NN}_\tau < 0.8$ (0.9) for the $\mu\tau jj$ ($e\tau jj$) analyses. The muon is selected by reversing at least one of the isolation criteria and the electron is selected by inverting the likelihood requirement. We subtract the estimated number of events contributed from other SM backgrounds in the MJ model sample, and compute the ratio ρ of the opposite-sign lepton-tau pairs to the same-sign pairs. We then multiply the number of events in our signal sample with same-sign pairs (after subtracting SM background) by ρ to obtain the number of expected MJ events in our opposite-sign signal sample. The ρ values are close to unity, and show no significant dependence on the p_T or η of the leptons or jets. The baseline MJ sample distributions (after subtraction of SM backgrounds) are used to model the distributions of multijet kinematic distributions.

To estimate the uncertainty in the MJ background, we employ two different models. In one, the lepton requirements are those for the signal sample, but the NN_τ requirement is lowered as for the baseline MJ sample. The other uses the NN_τ requirement as defined for the signal sample, but the lepton selection is the same as in the baseline MJ sample.

We have verified the method for establishing the multijet background determinations in the higher statistics $e\tau + 1$ jet and $\mu\tau + 1$ jet samples, selected in the same way for ‘signal’ and ‘MJ model’ as described above, apart from the requirement of having exactly one jet. Good agreement between data and predicted backgrounds is observed.

F. Other control samples

We have checked the modelling of the $W(\rightarrow \mu\nu)+$ jets background using data that requires $p_T^\mu > 25$ GeV, a τ with $NN_\tau < 0.9$, $\cancel{E}_T > 30$ GeV and 2 jets. This sample is about 85% pure $W+$ jets, and we find good agreement between the kinematic distributions of data and prediction from MC.

We select a 99% pure $Z(\rightarrow \mu\mu)+$ jets control sample by removing the τ requirement, and requiring two isolated muons with $p_T > 25$ GeV and two jets. The shapes of all kinematic distributions in data and predicted backgrounds are consistent.

G. Yields

The estimated number of events from all background sources and the number of observed data in our signal selection are given in Tables I and II. The fractions contributing to the total yield for each of the nine signal processes as a function of m_H is shown in Fig. 1 for the $\mu\tau jj$ and $e\tau jj$ analyses. The number of expected events from each of the nine sources of signal reactions at representative values of M_H 110, 130 and 160 GeV is given in Table III.

τ type	$t\bar{t}$	$W+$ jets	$Z_{\mu\mu}+$ jets	$Z_{\tau\tau}+$ jets	DB	MJ	Σ Bkgd	Data
type 1	7.9	5.7	2.9	17.9	1.3	11.4	47.2	56
type 2	65.7	37.5	16.7	108.8	8.3	40.4	277.6	287
type 3	8.3	21.6	2.7	27.7	1.6	18.2	80.2	71
All	82.0	64.8	22.3	154.5	11.3	70.0	404.9	414

TABLE I: The number of background events expected from SM processes, MJ background, and observed data, for individual and all tau types after preselection in the $\mu\tau jj$ analysis. “DB” stands for di-boson processes.

τ type	$t\bar{t}$	$W+$ jets	$Z_{ee}+$ jets	$Z_{\tau\tau}+$ jets	DB	MJ	Σ Bkgd	Data
type 1	2.3	2.9	0.6	6.3	0.6	6.0	18.8	10
type 2	14.9	21.8	17.2	30.9	1.5	32.0	118.4	117
type 3	7.2	17.8	2.0	11.4	1.4	21.7	61.1	61
All	24.4	42.6	19.8	48.6	3.6	59.2	198.3	188

TABLE II: The number of background events expected from SM processes, MJ background, and observed data, for individual and all tau types after preselection in the $e\tau jj$ analysis. “DB” stands for di-boson processes.

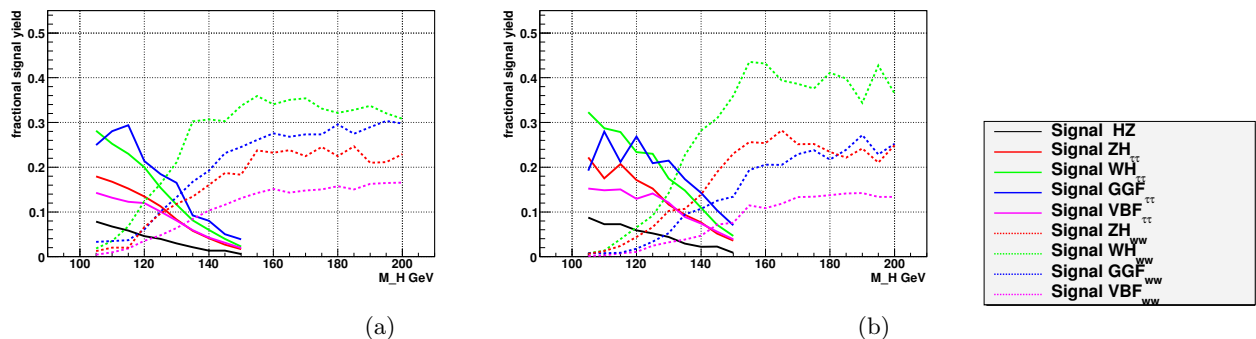


FIG. 1: Fractional yields for H signals as a function of M_H for (a) the $\mu\tau jj$ and (b) $e\tau jj$ analyses.

III. MULTIVARIATE ANALYSIS

As no single set of selections on kinematic variables suffices to discriminate signal from the background, we turn to multivariate techniques to attain better separation. We choose stochastic gradient boosted decision trees (BDT) [17]

m_H (GeV)	channel	HZ	$ZH_{\tau\tau}$	$WH_{\tau\tau}$	$GGF_{\tau\tau}$	$VBF_{\tau\tau}$	ZH_{WW}	WH_{WW}	GGF_{WW}	VBF_{WW}	Total
110	$\mu\tau jj$	0.075	0.186	0.279	0.311	0.146	0.022	0.038	0.038	0.011	1.11
	$e\tau jj$	0.034	0.081	0.133	0.130	0.069	0.006	0.006	0.004	0.001	0.464
130	$\mu\tau jj$	0.035	0.099	0.139	0.196	0.0959	0.140	0.251	0.158	0.075	1.189
	$e\tau jj$	0.017	0.044	0.067	0.082	0.046	0.039	0.054	0.020	0.012	0.381
160	$\mu\tau jj$	--	--	--	--	--	0.315	0.461	0.374	0.205	1.355
	$e\tau jj$	--	--	--	--	--	0.085	0.145	0.069	0.036	0.335

TABLE III: Number of events for each signal/decay process expected after preselection in the $\mu\tau jj$ and $e\tau jj$ analyses for selected Higgs boson masses.

as implemented in TMVA [18] for this purpose. The stochastic gradient BDT algorithm splits a sample of MC signal and background events into a tree structure, choosing at each splitting node the optimum cut on that variable which yields the best separation of signal and background in the ensuing two daughter nodes. The algorithm is recursive so that after each iteration, misclassified events are reweighted and the algorithm is tried again. Each splitting node uses a subset of the available events, and in successive iterations of the training a negative feedback is introduced to mitigate the effects of overtraining for poor statistics samples.

We choose a set of well-modelled kinematic variables for which the distributions of at least some signal and some background are different. The BDT algorithm does not degrade if variables yielding little signal over background separation are included. The input variables chosen are shown in Table IV.

variable	definition
p_T^ℓ	p_T of the lepton candidate
p_T^{j1}	p_T of the leading jet candidate
\cancel{E}_T	missing transverse energy
$M_{\tau\tau}$	invariant mass of the $(\tau_\ell, \tau_{\text{had}})$ system
M_{jj}	invariant mass of the two candidate jets
ΔR_{jj}	$\Delta R = \sqrt{(\Delta\phi)^2 + (\Delta\eta)^2}$ distance between the 2 leading jets
M_T^ℓ	transverse mass calculated from p_T^ℓ and \cancel{E}_T
M_T^τ	transverse mass calculated from p_T^τ and \cancel{E}_T
H_T	scalar sum of the p_T of all jets with $p_T > 15$ GeV and $ \eta < 2.5$
S_T	scalar sum of the p_T of ℓ, τ , the two jets and \cancel{E}_T
V_T	magnitude of the vector sum of the p_T of ℓ, τ , the 2 jets and \cancel{E}_T
$A(\cancel{E}_T, \cancel{H}_T)$	asymmetry between \cancel{E}_T and \cancel{H}_T , $(\cancel{E}_T - \cancel{H}_T) / (\cancel{E}_T + \cancel{H}_T)$. \cancel{H}_T is Σp_T^τ for jets
$\min \Delta\phi(\cancel{E}_T, jets)$	the smaller $\Delta\phi$ between the \cancel{E}_T and any jet
\mathcal{S}	the \cancel{E}_T significance [16]
$\Delta\eta(jj)$	$ \Delta\eta $ between the 2 leading jets
p_T^τ	transverse momentum of the tau candidate that decays $\tau \rightarrow \text{hadrons}$

TABLE IV: Variables used for the BDT training.

Representative distributions of input variables for BDT training are shown in Fig. 2.

This analysis considers nine signal processes (ZH, WH, GGF, VBF , all with $H \rightarrow \tau\tau$ or WW , and HZ with $H \rightarrow b\bar{b}$ $Z \rightarrow \tau\tau$), and four main backgrounds ($t\bar{t}, W + \text{jets}, Z + \text{jets}$ and MJ). Moreover there are three rather distinct regions of Higgs mass, $M_H < 125$, $125 \leq M_H \leq 135$ GeV and $M_H > 135$ GeV, in which the dominant production and decay processes are different. In principle we would wish to discriminate each of these signals from each of the backgrounds in all three mass regions, giving 108 separate multivariate trainings. This would be cumbersome, so we simplify the BDT analysis as follows:

Higgs mass region	Signals
low	$GGF_{\tau\tau}$ $VH_{\tau\tau}$ $VBF_{\tau\tau}$
intermediate	$GGF_{\tau\tau}$ GGF_{WW} $VH_{\tau\tau}$ VH_{WW}
high	GGF_{WW} VH_{WW} VBF_{WW}

TABLE V: Signals used for BDT training in the three Higgs boson mass ranges

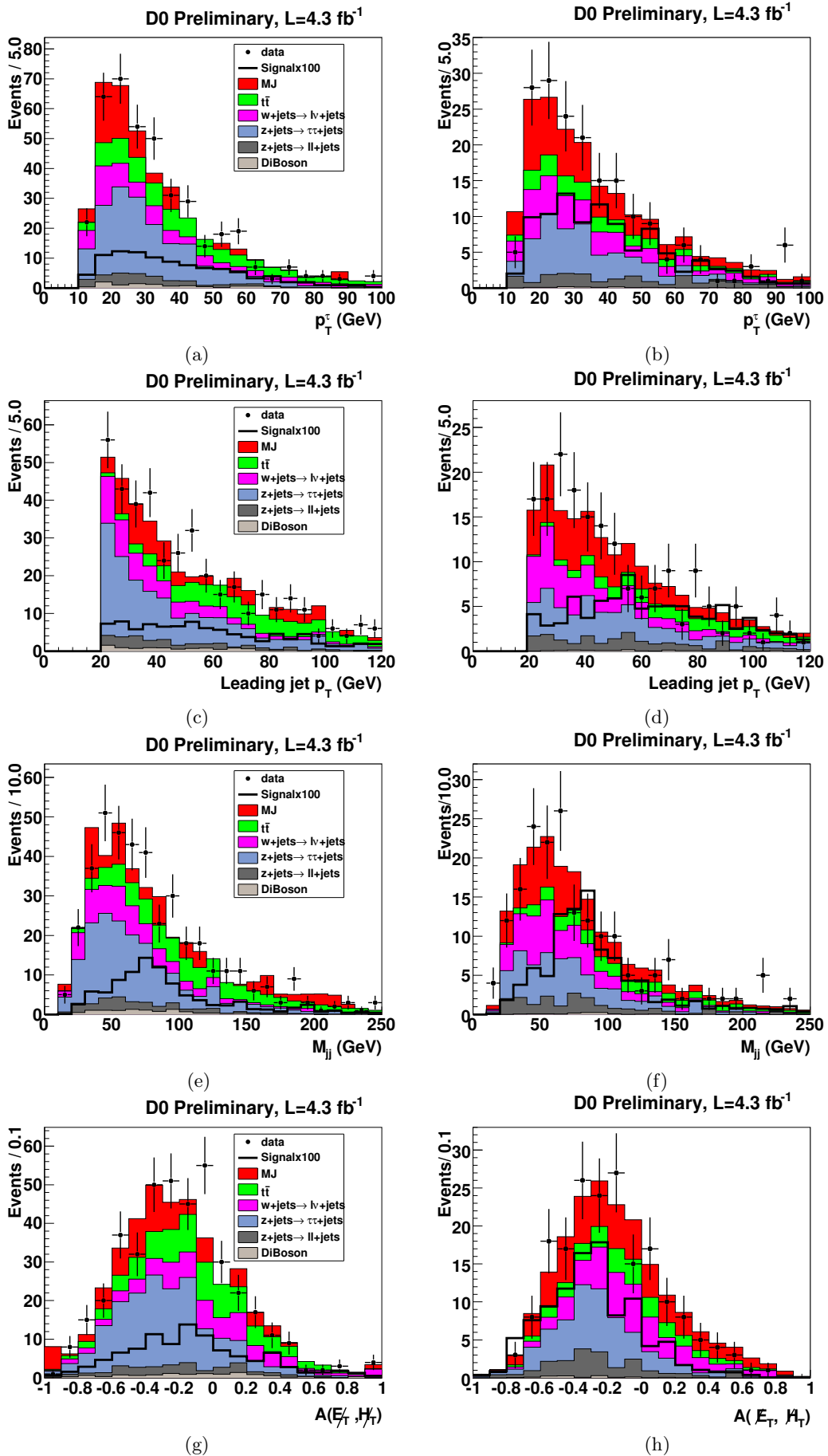


FIG. 2: Comparison of data and expected backgrounds for (a), (b) p_T^τ ; (c), (d) $p_T(\text{jet}_1)$; (e), (f) M_{jj} ; and (g), (h) $A(\not{E}_T, \not{H}_T)$. The signals are shown for $M_H = 115 \text{ GeV}$ and are multiplied by a factor of 100. Distributions are shown for $\mu\tau jj$ (left) and $e\tau jj$ (right).

- We note that the $t\bar{t}$ and $W + \text{jets}$ backgrounds have similar properties and so we merge these for BDT training;
- The WH and ZH signal processes are also similar and therefore we combine them as a common VH signal for BDT training;
- There are different dominant signals in each of the three M_H regions. So we train BDTs for only those that contribute at least 10% of the total signal in each mass region.

With these simplifications, the signal combinations that are trained against the three backgrounds ($t\bar{t}$ plus $W + \text{jets}$, $Z + \text{jets}$, and MJ) are shown in Table V.

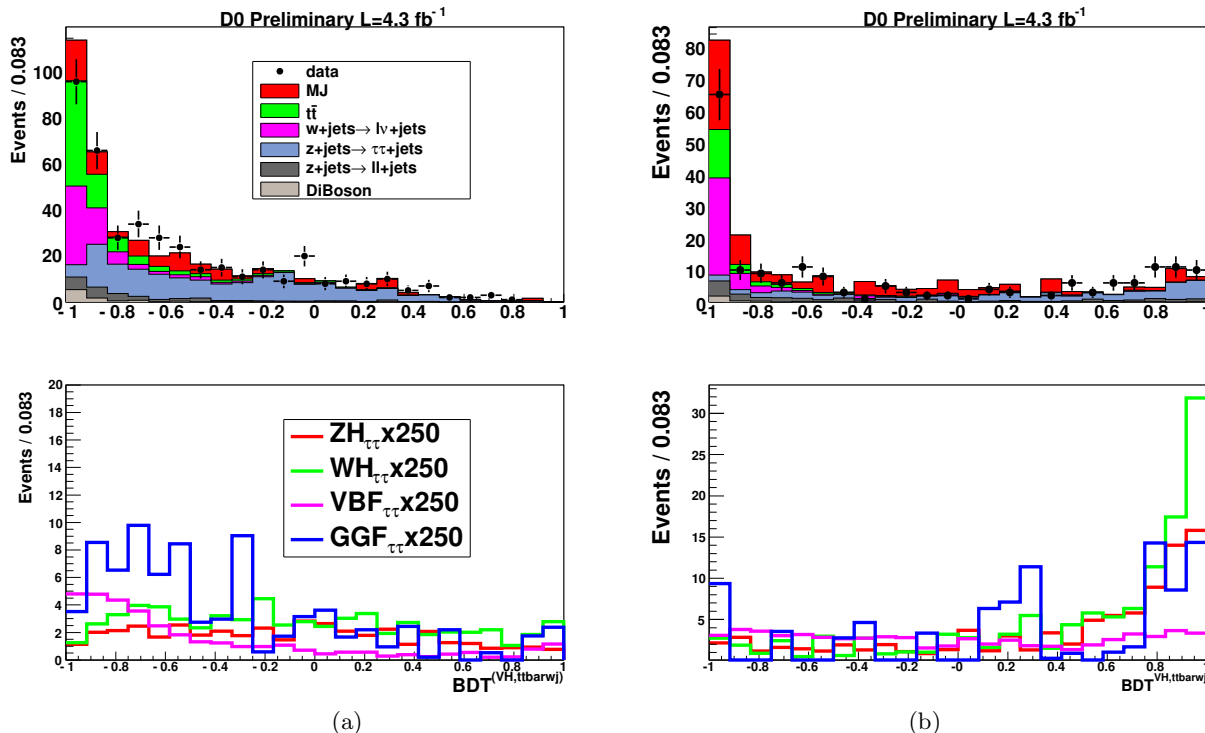


FIG. 3: Representative BDTs for $\mu\tau jj$ (a) and $e\tau jj$ (b) for WH and ZH signals trained against $t\bar{t}$ and $W + \text{jets}$ backgrounds in the low mass region. The signals are shown for $M_H = 115$ GeV and are multiplied by a factor of 250.

Representative BDT outputs for events trained on specific signals and backgrounds are shown in Figs. 3, 4 and 5. These distributions are typical in that the signal and background used in the training are well separated by the multivariate classifier. The signals (backgrounds) that are not used for the training sometimes fall in the low (high) regions of BDT output where backgrounds (signals) are expected to dominate. We therefore construct a final combined BDT (cBDT) in each mass region, using the individual BDT outputs in that region as inputs into the cBDT. The task of the cBDT is to weigh conflicting information, *e.g.* whether a particular event is more like one of the signals than any of the backgrounds.

In the $e\tau jj$ channel, we observe that in some cases the $Z + \text{jets}$ background events migrate to the high cBDT region, and we attribute this to the fact that the individual BDTs trained between VH or VBF signals and MJ background put the $Z + \text{jets}$ events at high BDT output values. Thus the cBDT is faced with conflicting information on whether these $Z + \text{jets}$ events are signal and background. We performed an optimization in which we successively dropped individual BDTs in the cBDT training and examined the change in expected Higgs production limits. From this optimization we choose to drop the VH vs MJ and VBF vs MJ BDTs in the low mass $e\tau jj$ cBDT and all three signals vs MJ background BDTs in the high mass $e\tau jj$ cBDT. The final cBDT distributions are shown in Fig. 6.

IV. SYSTEMATIC UNCERTAINTIES

Some of the systematic uncertainties do not modify the shape of the cBDT distribution and these are termed ‘flat’. Others which do modify the shape are denoted as ‘shape’. Systematic uncertainties for each factor that influences the

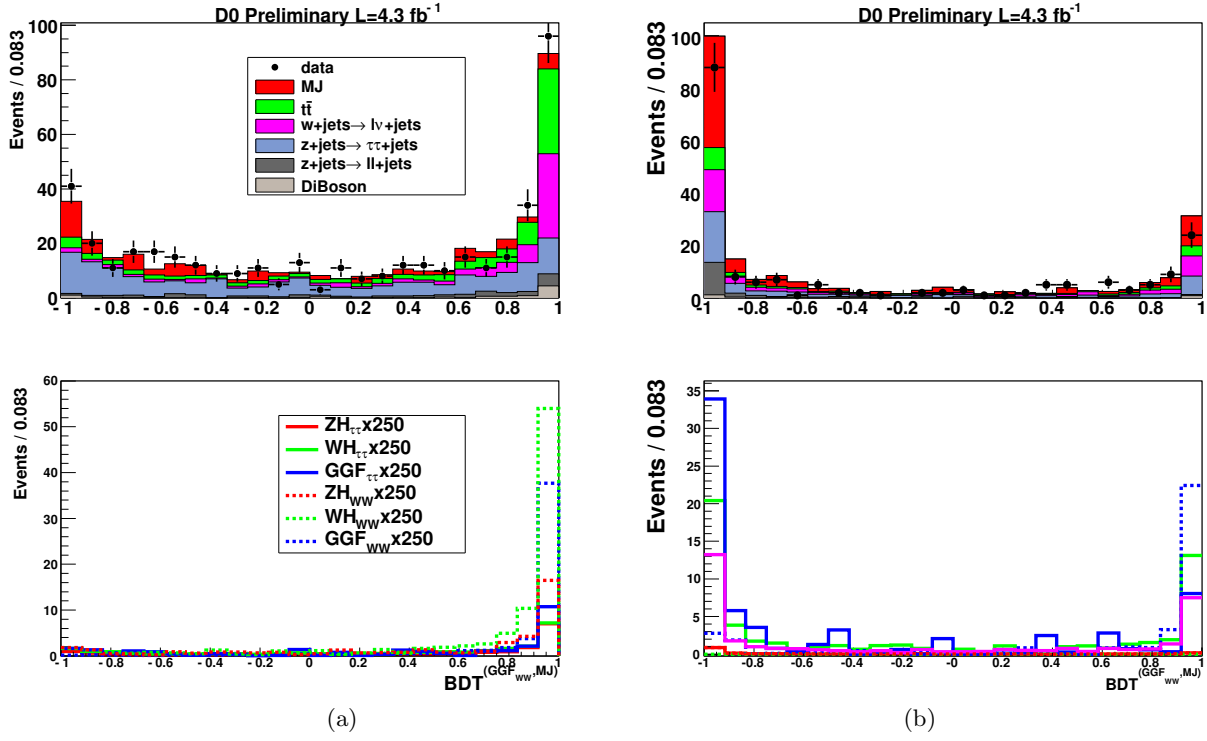


FIG. 4: Representative BDTs for $\mu\tau jj$ (a) and $e\tau jj$ (b) for GGF_{WW} signal trained against multijet background in the intermediate mass region. The signals are shown for $M_H = 135$ GeV and are multiplied by a factor of 250.

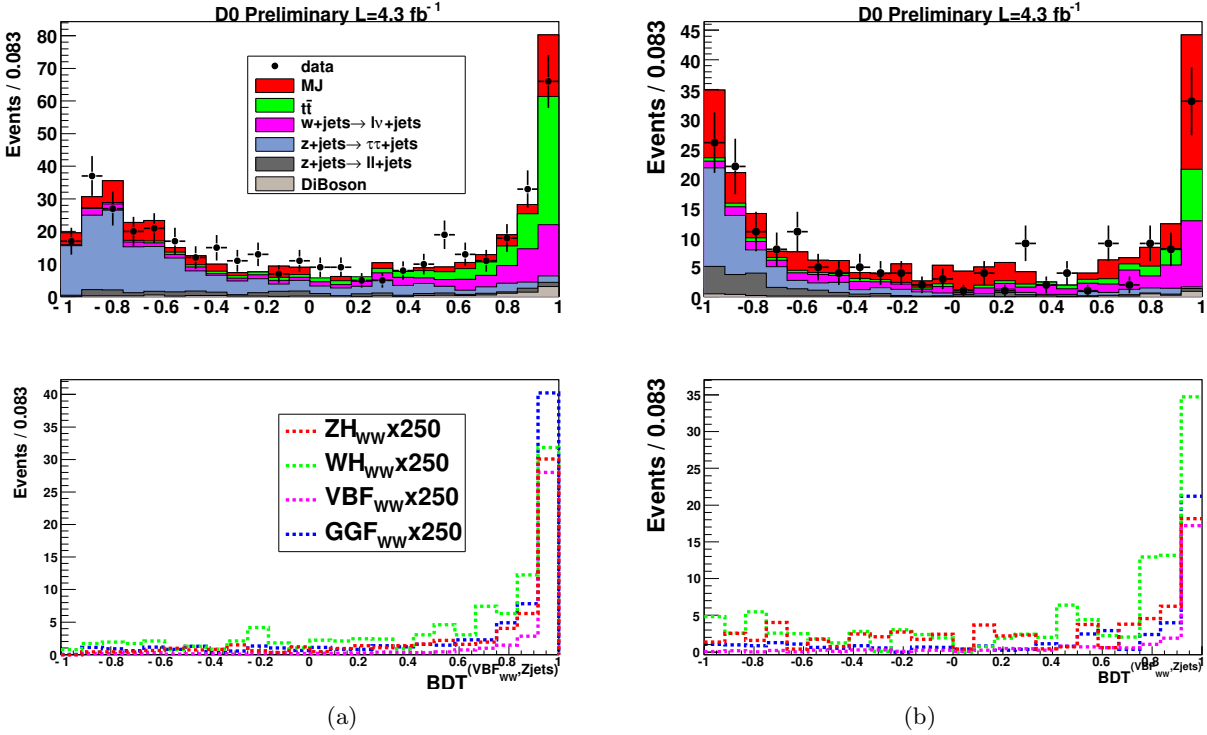


FIG. 5: Representative BDTs for $\mu\tau jj$ (a) and $e\tau jj$ (b) for VBF_{WW} signal trained against $Z + \text{jets}$ background in the high mass region. The signals are shown for $M_H = 165$ GeV and are multiplied by a factor of 250.

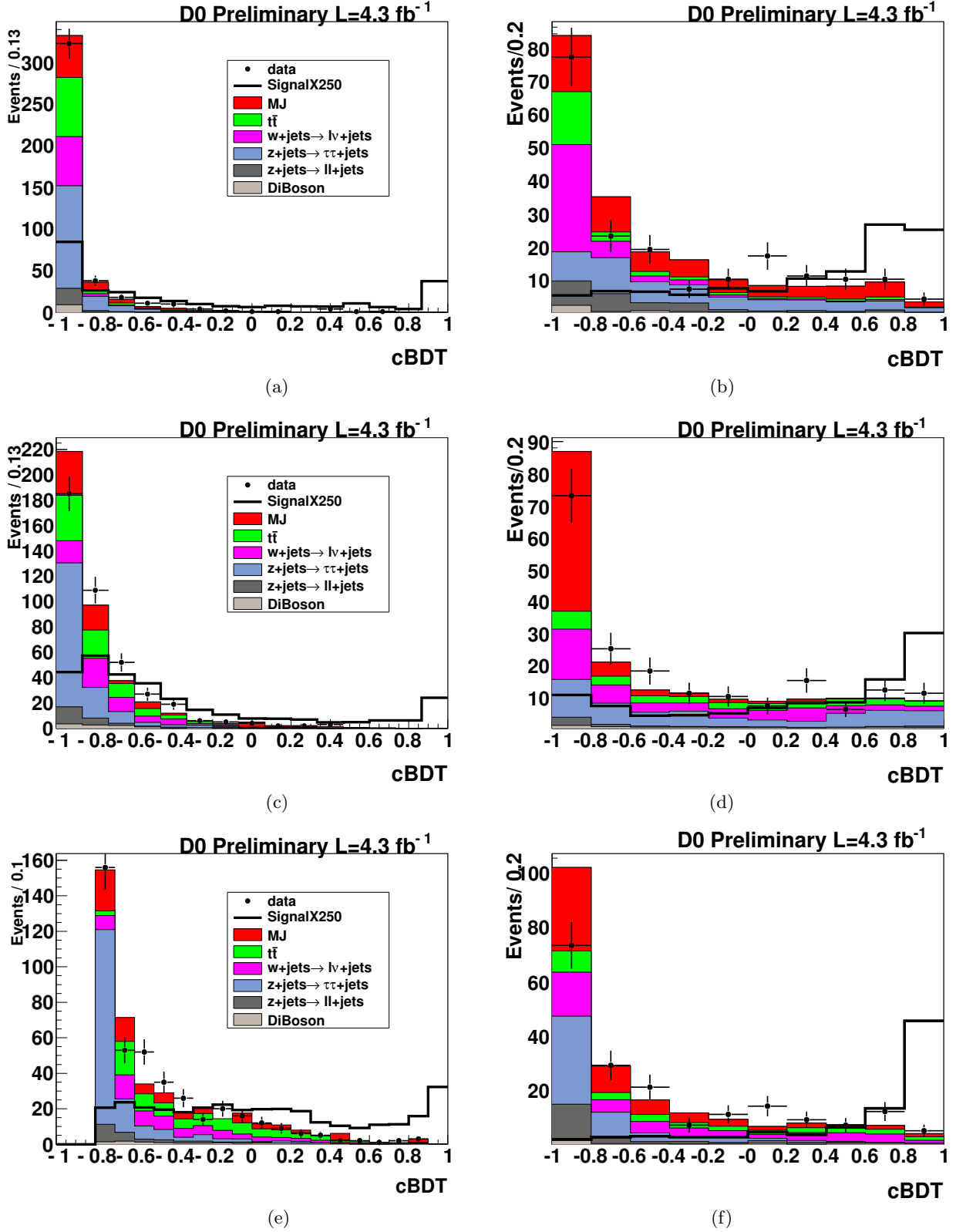


FIG. 6: Combined BDTs for $\mu\tau jj$ (left) and $e\tau jj$ (right) for: (a), (b) low Higgs mass region; (c), (d) intermediate Higgs mass region; (e), (f) high Higgs mass region. The signals in the (low, intermediate and high) mass region are shown for $M_H = (115, 135 \text{ and } 165) \text{ GeV}$ and are multiplied by a factor of 250.

Source	type	Uncertainty (%)
Luminosity ($D\bar{O}$ specific)	flat	4.1
Luminosity (Tevatron common)	flat	4.6
μ ID, track match, iso.	flat	2.9
μ trigger	flat	8.6
e ID, track match, iso.	flat	4
e trigger	flat	2
τ energy correction	flat	9.8
τ track efficiency	flat	1.4
τ selection types 1,2,3	flat	12, 4.2, 7
W/Z +light flavor XS	flat	6.0
$t\bar{t}$, single top XS	flat	10.0
diboson XS	flat	7.0
VH signal XS	flat	6.2
VBF signal XS	flat	4.9
GGF signal XS normalization	flat	33
GGF signal XS PDF	flat	29
GGF p_T^H	shape	1.0
vertex confirmation for jets	flat	4.0
Jet ID/reco eff.	shape	$\approx 20\%$
Jet E resolution.	shape	$\approx 15\%$
JES	shape	$\approx 15\%$
jet p_T	flat	5.5
PDF	shape	2.0
MJ $\mu\tau jj$ normalization	flat	5.3
MJ $e\tau jj$ normalization	flat	4.7
MJ shape ($\mu\tau jj$)	shape	15%
MJ shape ($e\tau jj$)	shape	15%

TABLE VI: Systematic uncertainties (in percent) on the final cBDT.

final cBDT distributions are estimated by changing the relevant factor by ± 1 standard deviation from its nominal value and propagating the change to the cBDT distribution. In the case of the multijet background uncertainty which is taken from data, we modify the choice of the MJ model either by modifying the NN_τ selection or the lepton selection, but not both as for the baseline MJ model sample described above. These two alternates are used as the upward and downward changes which are input to the cBDT calculation to obtain the MJ background systematic uncertainty. While most of the systematic uncertainties affect all three Higgs mass regions in the same way, those involving jet energy scale, jet energy resolution, jet ID and reconstruction, and the multijet background, are recomputed in each mass region. Table VI lists the systematic uncertainties, whether they are flat or shape-dependent, and their relative size. For the shape-dependent systematics, the value shown corresponds to an approximate average across the bins of the cBDT distributions.

V. LIMIT CALCULATION

The upper limits on the production cross section of Higgs bosons assuming SM Higgs decay branching ratios are calculated using the modified frequentist method [19]. The test statistic is the negative of a binned Poisson log-likelihood ratio (LLR) computed at each of the assumed Higgs mass values from 105 to 200 GeV in 5 GeV steps. Since the statistics for this search are small, fluctuations in signal or background event samples can affect the limits. We have optimized the bin sizes for the best expected limits and choose values (0.133, 0.133 and 0.1) for the $\mu\tau jj$ channel in the (low, intermediate and high mass regions) and (0.2, 0.2, and 0.2) for the corresponding $e\tau jj$ bin sizes. For the $\mu\tau jj$ analysis, there is very little background near $cBDT = +1$, so to give stability in the limit setting we merge the final (2, 3, and 2) bins for the (low, intermediate, and high) mass regions. The LLR for different hypotheses (*e.g.* background-only, LLR_b , or signal+background, LLR_{s+b}) are used to compute the confidence levels CL_b and CL_{s+b} that give the probability that the LLR value from a set of 50,000 simulated pseudo-experiments is less likely than that observed, at a given confidence level.

The cross sections of the hypothesized Higgs signal at a given M_H are then scaled up from their SM values until the value of $CL_s = CL_{s+b}/CL_b$ reaches 0.05 which defines the limit cross sections at 95% CL. In the calculation, all contributions to systematic uncertainty are fitted, subject to the constraints given on their estimated uncertainties, to yield the best fit. Correlations of systematic uncertainties among signal and/or background processes are accounted for in the minimization. The expected and observed limits for are shown in Figs. 7, 8 and 9 for the $\mu\tau jj$ and $e\tau jj$

channels from this analysis separately and for the combination of these two channels together with the limits in the $\mu\tau jj$ channel computed previously [1]. The prior 1 fb^{-1} analysis [1] considered only the signals with $H \rightarrow \tau\tau$ and within the search range $105 < M_H < 150 \text{ GeV}$. Since that analysis computed limits from 105 to 145 GeV in 10 GeV intervals, we averaged the inputs from the neighboring mass points to supply the missing inputs for the combination. The expected LLRs for signal + background and background only (with ± 1 and ± 2 standard deviation bands for LLR_b) and the observed LLR are also shown in Figs. 7, 8 and 9. The 95% C.L. limits for are given in Table VII for the $4.3 \text{ fb}^{-1} \mu\tau jj, e\tau jj$ channels, and the combination of both with the previous 1.0 fb^{-1} analysis.

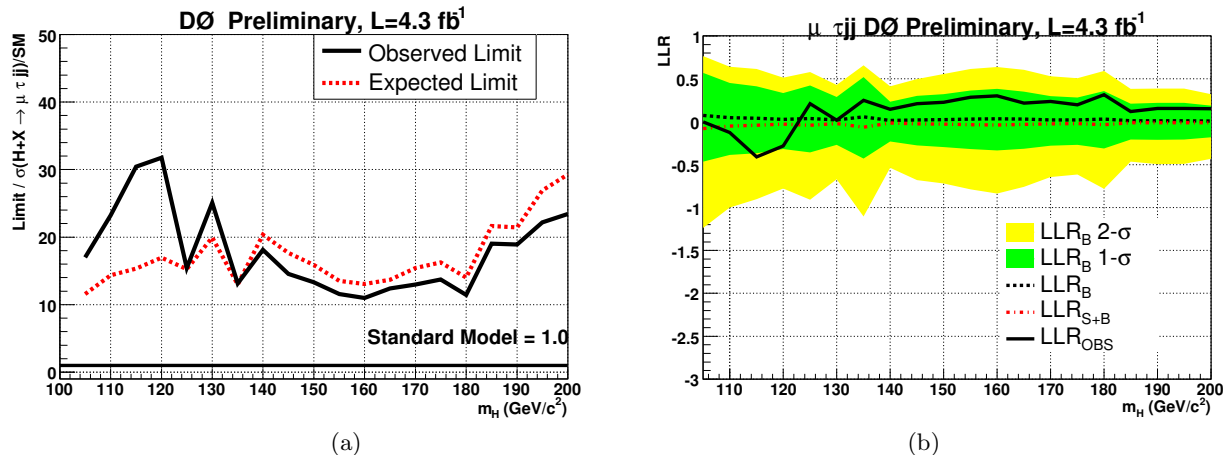


FIG. 7: For the $4.3 \text{ fb}^{-1} \mu\tau jj$ analysis, (a) ratio of the 95% upper C.L. limits to the SM cross section and (b) LLR, as functions of Higgs boson mass.

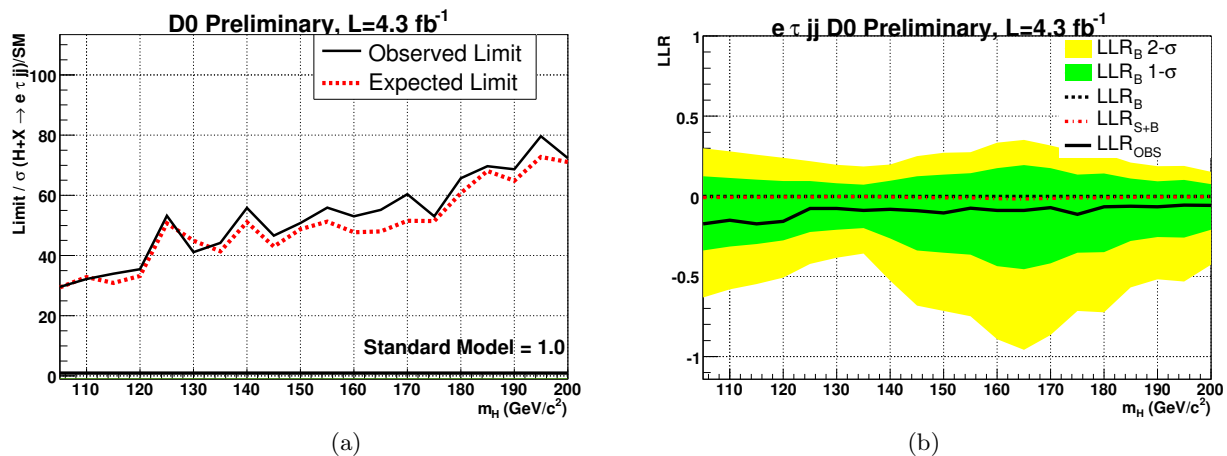


FIG. 8: For the $4.3 \text{ fb}^{-1} e\tau jj$ analysis, (a) ratio of the 95% upper C.L. limits to the SM cross section and (b) LLR, as functions of Higgs boson mass.

VI. CONCLUSION

We have searched for SM Higgs boson production in final states containing an electron or muon, a hadronically decaying tau plus two jets. This final state is reached from several different Higgs production processes and decay modes. For the Higgs boson mass range $105 \leq M_H \leq 200 \text{ GeV}$ the 95% C.L. limits are relatively insensitive to the Higgs mass owing to the sensitivity to both $H \rightarrow \tau\tau$ and $H \rightarrow WW$ decay modes. The expected and observed upper limits for are shown in Table VII and for the $4.3 \text{ fb}^{-1} \mu\tau jj, e\tau jj$ results and the combination of both with the previous 1.0 fb^{-1} analysis in Figs. 7, 8 and 9 respectively. At $M_H = 110, 130$ and 160 GeV , after combining the results in this analysis with that of a previous publication [1], we set a final combined limit on SM Higgs boson production that is

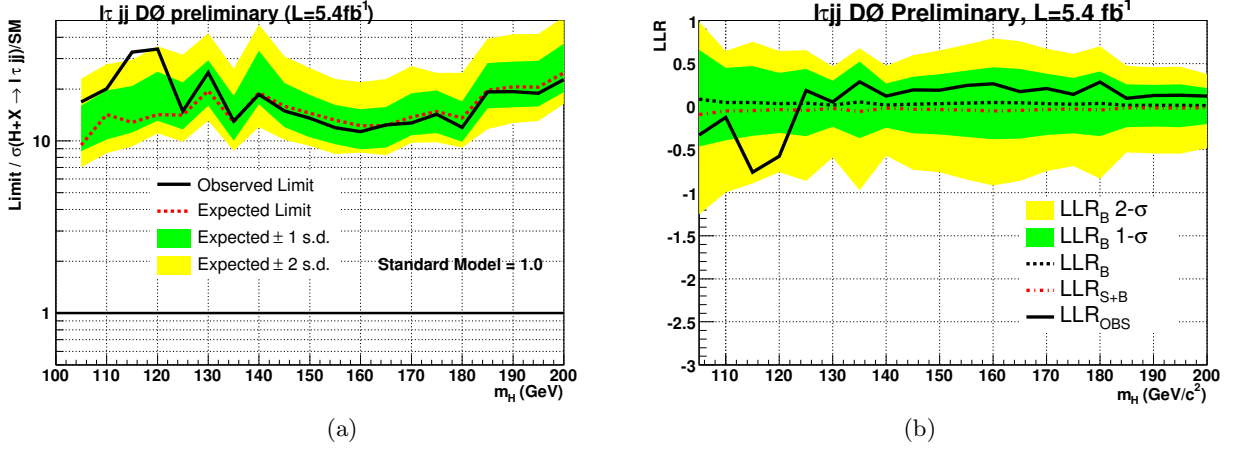


FIG. 9: For the combined 4.3 fb⁻¹ $\mu\tau jj$ and $e\tau jj$ analyses, and the 1.0 fb⁻¹ $\mu\tau jj$ analysis of Ref. [1], (a) ratio of the 95% upper C.L. limits to the SM cross section and (b) LLR, as functions of Higgs boson mass. The shaded bands show the 1 and 2 σ uncertainties relative to the expected background only values.

m_H (GeV)	$\mu\tau jj$		$e\tau jj$		combined	
	exp	obs	exp	obs	exp	obs
105	11.6	17.0	29.4	29.6	9.4	16.8
110	14.3	23.2	32.8	32.2	14.0	20.1
115	15.3	30.4	30.9	34.0	12.8	32.8
120	17.0	31.8	33.3	35.4	14.2	34.1
125	15.3	15.4	50.7	53.2	14.1	14.8
130	20.0	25.1	44.9	41.1	19.5	24.2
135	13.0	13.1	41.4	44.2	12.9	13.0
140	20.4	18.1	51.0	55.8	19.1	18.6
145	17.7	14.6	43.0	46.7	15.9	14.9
150	15.9	13.3	48.8	50.8	14.5	13.5
155	13.5	11.6	51.3	56.0	13.2	11.9
160	13.1	11.0	47.7	53.1	12.2	11.3
165	13.7	12.4	48.0	55.2	12.3	12.4
170	15.4	13.0	51.5	60.4	13.7	12.7
175	16.2	13.7	51.5	53.1	14.8	14.3
180	14.0	11.4	60.7	65.7	13.6	12.0
185	21.6	19.0	68.1	69.6	19.7	19.3
190	21.4	18.9	64.9	68.7	20.6	19.3
195	26.9	22.2	72.7	79.6	20.5	18.9
200	29.3	23.4	71.0	72.4	24.8	22.6

TABLE VII: Ratio of the 95% CL cross section limits to the SM predictions. The $\mu\tau jj$ and $e\tau jj$ columns are from this analysis. The combined limits include the combination of $\mu\tau jj$ and $e\tau jj$ channels from this analysis with the previous $\mu\tau jj$ from Ref [1].

a factor of 20, 24, and 11 times larger than the cross section predicted in the SM, to be compared to the expected ratios of 14, 20 and 12.

We thank the staffs at Fermilab and collaborating institutions, and acknowledge support from the DOE and NSF (USA); CEA and CNRS/IN2P3 (France); FASI, Rosatom and RFBR (Russia); CNPq, FAPERJ, FAPESP and FUNDUNESP (Brazil); DAE and DST (India); Colciencias (Colombia); CONACyT (Mexico); KRF and KOSEF (Korea); CONICET and UBACyT (Argentina); FOM (The Netherlands); STFC (United Kingdom); MSMT and GACR (Czech Republic); CRC Program, CFI, NSERC and WestGrid Project (Canada); BMBF and DFG (Germany); SFI (Ireland); The Swedish Research Council (Sweden); CAS and CNSF (China); and the Alexander von Humboldt Foundation (Germany).

-
- [1] V.M. Abazov *et al.*, (D0 Collaboration), Phys. Rev. Lett **102**, 251801 (2009).
 - [2] The DØ collaboration, <http://www-d0.fnal.gov/Run2Physics/WWW/results/prelim/HIGGS/H79/H79.pdf>.
 - [3] V.M. Abazov *et al.*, (D0 Collaboration), Nucl. Instrum. Methods Phys. Res A **565**, 463 (2006).
 - [4] V.M. Abazov *et al.*, (D0 Collaboration), Nucl. Instrum. Methods Phys. Res A **552**, 372 (2005).
 - [5] T. Sjöstrand *et al.*, Computer Phys. Commun. **135**, 238 (2001); T. Sjöstrand *et al.*, arXiv:(hep-ph) 0108264 (2001).
 - [6] J. Pumplin *et al.*, J. High Energy Phys. **07**, 12 (2002).
 - [7] C. Anastasiou, R. Boughezal and F. Petriello, J. High Energy Phys. **04**, 003 (2009); D. de Florian and M. Grazzini, Phys. Lett. B **674**, 291 (2009); K.A. Assamagan *et al.*, arXiv:hep-ph/0406152; O. Brein, A. Djouadi and R. Harlander, Phys. Lett. B **579**, 149 (2004); M.L. Ciccolini, S. Dittmaier and M. Krämer, Phys. Rev. D **68**, 073003 (2003); E.L. Berger and J. Campbell, Phys. Rev. D **90**, 073011 (2004).
 - [8] M. Mangano *et al.*, J. High Energy Physics **0307**, 001 (2003).
 - [9] A. Djouadi, J. Kalinowski, M. Spira, arXiv: (hep-ph) 9704448 (1997).
 - [10] S. Jadach *et al.*, Computer Phys. Commun. **76**, 361 (1993).
 - [11] J. Campbell and K. Ellis, <http://mcfm.fnal.gov/>.
 - [12] R. Brun and F. Carminati, CERN Program Library Long Writeup W5013, 1993 (unpublished), version V3.21.
 - [13] V.M. Abazov *et al.* (D0 Collaboration), Phys. Rev. D **71**, 072004 (2005).
 - [14] G. Blazey *et al.*, in *Proceedings of the Workshop: QCD and Weak Boson Physics in Run II*, edited by U. Baur, R.K. Ellis and D. Zeppenfeld, Fermilab-Pub-00/297 (2000).
 - [15] V.M. Abazov *et al.* (D0 Collaboration), Phys. Rev. Lett. **105**, 251801 (2010).
 - [16] A. Schwartzman, Fermilab-THESIS-2004-21.
 - [17] L. Breiman *et al.*, *Classification and Regression Trees* (Wadsworth, Stamford CT, 1984); D. Bowser-Chao and D.L. Dzialo, Phys. Rev D **47**, 1900 (1993).
 - [18] TMVA Users Guide, CERN-OPEN-2007-007 and arXiv:physics/0703039.
 - [19] A. Read, J. Phys. G: Nucl. Part. Phys. **28**, 2693 (2002); T. Junk, Nucl. Instrum. Methods A **434**, 435 (1999).